



Highly improved predictive skill in the forecasting of the East Asian summer monsoon

Eungul Lee,^{1,2,3} Thomas N. Chase,^{1,4} and Balaji Rajagopalan^{1,4}

Received 11 September 2007; revised 23 July 2008; accepted 4 August 2008; published 29 October 2008.

[1] The East Asian summer monsoon greatly influences the lives and property of about a quarter of the people in the world. However, the predictive skill of the monsoon is very low in comparison with that of the Indian summer monsoon because of the complexity of the system which involves both tropical and subtropical climates. Previous monsoon prediction models emphasized ocean factors as the primary monsoon forcing. Here we show that pre-season land surface cover is at least as important as ocean indices. New statistical forecast models of the East Asian summer monsoon using land cover conditions in addition to ocean heat sources double and triple, respectively, the predictive skill of the northern and southern East Asian summer monsoon forecasting models relative to models using ocean factors alone. This work highlights the, as yet, undocumented importance of seasonal land cover in monsoon prediction and the role of the biosphere in the climate system as a whole. We also detail the physical mechanisms involved in these land surface forcings.

Citation: Lee, E., T. N. Chase, and B. Rajagopalan (2008), Highly improved predictive skill in the forecasting of the East Asian summer monsoon, *Water Resour. Res.*, 44, W10422, doi:10.1029/2007WR006514.

1. Introduction

[2] The East Asian summer monsoon (EASM) involves both tropical and subtropical/midlatitude weather systems including cross-equatorial airflow and the Mei-yu, Changma and Baiu frontal zones [e.g., *Tao and Chen*, 1987; *Chang et al.*, 2000; *Wu and Wang*, 2002; *Wang and Li*, 2004; *Lee et al.*, 2005; *Lee et al.*, 2008a]. The complexity of these varied influences has resulted in low predictive skill in the forecasting of the EASM. In this study, we consider the regions of the northern and southern EASM (NEASM, 30°~50°N and 110°~145°E, and SEASM, 20°~30°N and 110°~145°E; see Figure 1a) covering eastern China, the Korean peninsula, Japan, and the adjacent marginal seas [*Lee et al.*, 2005; *Lee et al.*, 2008a].

[3] Physical properties of the land surface of the Asian continent may directly and indirectly affect the EASM circulations by affecting the land-sea heat contrast [e.g., *Webster*, 1987] as well as by supplying moisture through the southwesterly airflow passing southern Asia, originating in the Indian monsoon region and northern Australia and its neighboring sea regions [e.g., *Yihui*, 1994]. For example, *Meehl* [1994] used a number of general circulation model simulations to examine the influence of the land surface in the Indian summer monsoon and concluded that lower land-

surface albedo contributed to a greater land-sea temperature contrast and a stronger Indian summer monsoon due to warmer land temperatures. Land-surface conditions can also be associated with positive internal soil moisture feedback, i.e., a moisture source for reinforcing monsoon rainfall. Prior studies suggested that land use/land cover changes over the subtropics, i.e., Mongolia [*Xue*, 1996], east China [*Fu*, 2003], and Indochina peninsula [*Sen et al.*, 2004], could impact on the EASM. While these model simulations indicate the importance of land cover changes, no observational support for these model results has been reported. Here, we extend *Lee et al.* [2008a] by applying the linear regression framework used to develop the EASM forecast models using ocean factors alone to that using both ocean and land factors. The major objectives of this study are (1) to determine the relationships between EASM rainfall and vegetation activity in the surrounding regions that influence monsoon strength; (2) to provide plausible physical mechanisms to explain the relationships; (3) to determine the relative influence of land and ocean factors on the monsoon; and (4) to facilitate better seasonal forecasting of the sub-EASMs in terms of adding land cover indices.

2. Data and Methodology

2.1. Data

[4] Normalized Difference Vegetation Index (NDVI) observations are obtained from the NOAA Pathfinder Advanced Very High Resolution Radiometer (AVHRR) products [*Tucker et al.*, 2005] (downloaded from http://iridl.ldeo.columbia.edu/expert/SOURCES/UMD/GLCF/GIMMS/.NDVIg/global/ndvi/streamrescale/-999/setmissing_value/dods) and are used as an index for land cover. AVHRR NDVI data have been used extensively since 1981 to study a variety of global land processes [e.g., *Townshend*, 1994;

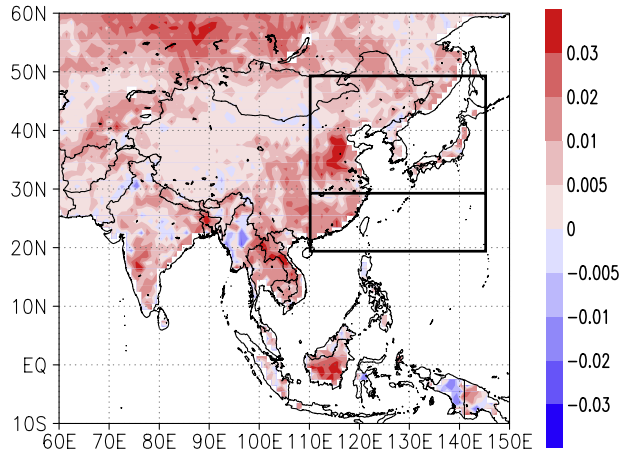
¹Cooperative Institute for Research in Environmental Sciences, University of Colorado, Boulder, Colorado, USA.

²Department of Geography, University of Colorado, Boulder, Colorado, USA.

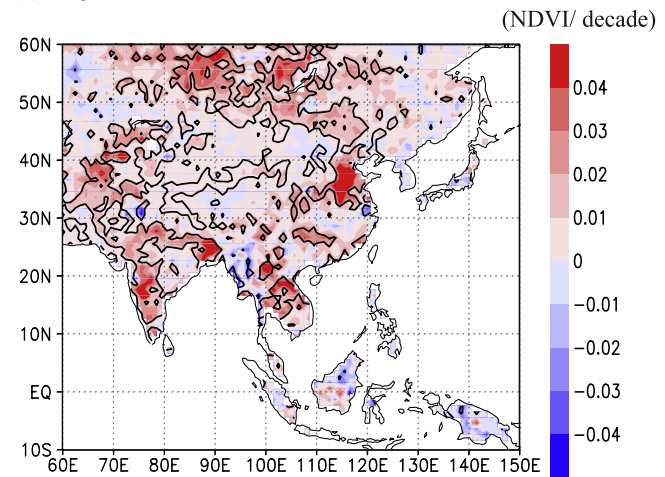
³Center for Sustainability and the Global Environment, University of Wisconsin, Madison, Wisconsin, USA.

⁴Department of Civil, Environmental, and Architectural Engineering, University of Colorado, Boulder, Colorado, USA.

(a) EOF 1 of MAM NDVI



(c) Regression trend of MAM NDVI



(b) PC 1 of MAM NDVI

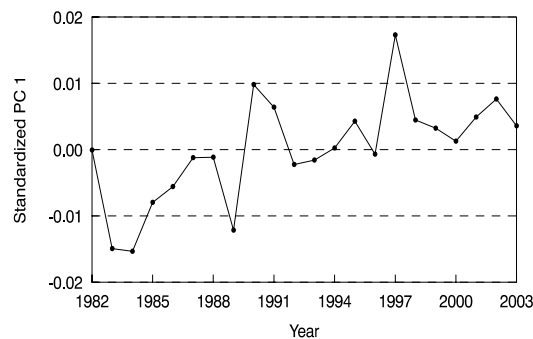


Figure 1. (a) EOF 1 (15.02% Var.) and (b) the corresponding standardized PC time series of MAM NDVI anomalies for 1982~2003 over Asia, i.e., 10°S~60°N and 60~150°E. Anomalies are area-weighted values. The upper and lower boxes in Figure 1a denote the NEASM and SEASM regions. (c) Spatial distribution of 1982~2003 regression trend of MAM NDVI (NDVI/decade). Significant regions at the 90% are contoured.

D'Souza et al., 1996; Cracknell, 1997; Defries and Belward, 2000; Biggs et al., 2006; Leavitt et al., 2008). It is also consistent and quantitatively compatible with the new generation global land surface satellite sensor data available from SPOT-4's Vegetation instrument (May 1998~present) and NASA's Moderate Resolution Imaging Spectrometers (MODIS) on the Terra and Aqua platforms (January 2000~present and December 2002~present, respectively) [*Tucker et al., 2005*]. NDVI is the unitless difference between near-infrared (channel 2) and red (channel 1) spectral reflectance normalized by their sum [*Tucker et al., 2005*].

[5] The NDVI is calculated as

$$\text{NDVI} = \frac{\text{channel 2} - \text{channel 1}}{\text{channel 2} + \text{channel 1}} \quad (1)$$

Spectral vegetation indices are highly correlated with the photosynthetically active biomass, chlorophyll abundance, and energy absorption [*Myneni et al., 1995*], so NDVI is a measure of green leaf density.

[6] Observed precipitation (mm/d) is derived from the Global Precipitation Climatology Project version 2 (GPCP) [*Adler et al., 2003*] and is used to calculate EASM rainfall for June through August (JJA), which are the three months with maximum monsoon intensity. In order to determine the influence of vegetation activity during the preceding spring (March, April, and May; MAM) on atmospheric dynamics during summer, we use upper-level divergence (s^{-1}) calculated with mean 150 hPa u - and v -winds (m/s) from the National Centers for Environmental Prediction-Department of Energy (NCEP-DOE) Atmospheric Model Intercomparison Project (AMIP-II) reanalysis [*Kanamitsu et al., 2002*]. To examine the physical mechanisms linking vegetation activity to monsoon circulation, we use latent heat flux [LHF (W/m^2)], sensible heat flux [SHF (W/m^2)], 2m temperature, volumetric soil moisture [fraction] between 0 and 10 cm below ground level (BGL), and 850 hPa wind vector (m/s) from NCEP-DOE AMIP-II reanalysis. For oceanic heat sources as potential predictors of EASM rainfall, we use sea surface temperature [SST ($^{\circ}\text{C}$)] from Hadley center [*Rayner et al., 2003*] and ocean heat content [OHC ($10^9 \text{ J}/\text{m}^2$)] from Scripps Institution of Oceanography

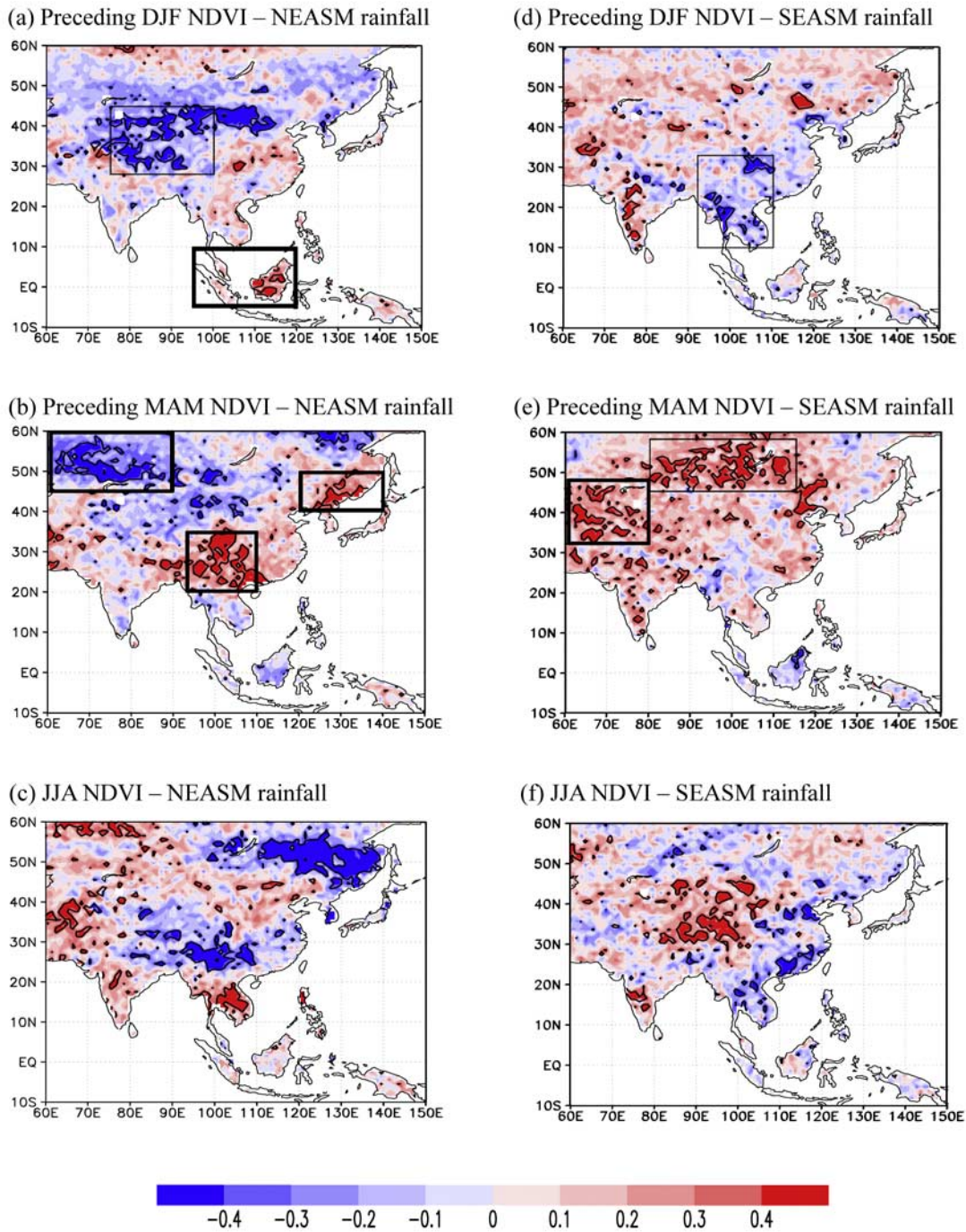


Figure 2. Correlation patterns of area-averaged JJA rainfall over the (left) NEASM and (right) SEASM regions with seasonal NDVIs. The boxes indicate the regions where potential predictors are calculated over. The regions for selected predictors are shown in bold boxes. Significant regions at the 90% level are contoured.

[White *et al.*, 2001]. OHC was calculated by depth for 11 levels (0~400 m), hence, it can express the characteristic of three-dimensional ocean [Lee *et al.*, 2008a].

[7] NDVI data are available from July 1981 and OHC data are only available through December 2003, so we examine 22 years from 1982 to 2003. Spatial resolutions (longitude \times latitude) of the data sets are $1^\circ \times 1^\circ$ for NDVI (converted from $0.073^\circ \times 0.073^\circ$) and SST, $2.5^\circ \times 2.5^\circ$ for GPCP and NCEP-DOE AMIP-II, and $5^\circ \times 2^\circ$ for OHC

data. In order to check the spatial consistency of the different gridded/interpolated data sets, we regridded the spatial resolution of NDVI to that of GPCP and NCEP-DOE data, and performed same statistical analyses used in this study. The results using the regridded NDVI (i.e., $2.5^\circ \times 2.5^\circ$) are consistent with those using higher resolution NDVI (i.e., $1^\circ \times 1^\circ$) (figures not shown), and the correlations between area-averaged NDVI anomalies over the boxes in Figure 2 from the two different resolution data

are very strong ($r > 0.9$; significant at 99%). We use the higher resolution NDVI that can show better vegetation information over East Asia than the lower resolution NDVI, especially over the Korean peninsula and Japan where the lower one could not give any NDVI information. To assess data consistency of OHC from SIO and SST from Hadley center, we compared SIO ocean temperature at 0 m (i.e., SST) with Hadley SST using the time series of annual mean SSTs area-averaged over the Tropic (i.e., $20^{\circ}\text{S}\sim 20^{\circ}\text{N}$ and $0^{\circ}\sim 360^{\circ}\text{E}$), where EASM rainfall has a significant correlation with SST anomalies, during 1955~2002. The time series of SIO SST are significantly correlated with those of Hadley SST ($r^2 = 0.9$).

[8] Winds from reanalyses are strongly constrained by observational data, but surface fluxes and soil moisture are calculated by the reanalysis model to be consistent with observed atmospheric fields [Kalnay *et al.*, 1996]. 2m temperature is influenced by both observational data and model. As point observations of surface flux, soil moisture, and near-surface air temperature are unavailable over the domain of our study, we use those from NCEP-DOE AMIP-II reanalysis. Surface flux data from NCEP-DOE AMIP-II have been used previously for large-scale climatic studies over Asia [e.g., Tomita *et al.*, 2007; Lee *et al.*, 2008b] and soil moisture from NCEP-DOE AMIP-II exhibited the highest correlation with observations among the three soil moisture reanalyses (i.e., European Centre for Medium-Range Weather Forecasts, NCEP-National Center for Atmospheric Research, and NCEP-DOE AMIP-II) [Li *et al.*, 2005].

2.2. Statistical Methods

[9] The first leading empirical orthogonal function (EOF 1) and its corresponding standardized principal component 1 (PC 1) of MAM NDVI anomalies (deviations from their 1982~2003 means) are used to examine land cover change in the Asian continent ($10^{\circ}\text{S}\sim 60^{\circ}\text{N}$ and $60\sim 150^{\circ}\text{E}$). In order to determine the relationship between EASM rainfall and seasonal NDVI anomalies, the spatial pattern of the correlation between EASM rainfall and seasonal NDVI anomalies is examined. We also use the composite analysis of JJA rainfall and 150 hPa divergences; for the NEASM- the 5 highest (1990, 1991, 1994, 1995, and 1997) and the 5 lowest (1985, 1989, 1993, 1996, and 1998) years of MAM NDVI in northern Asia (NA; $45\sim 60^{\circ}\text{N}$ and $60\sim 90^{\circ}\text{E}$), and for the 5 highest (1987, 1990, 1991, 1993, and 1998) and the 5 lowest (1984, 1985, 1988, 1989, and 1994) years of MAM NDVI in southern Asia (SA; $20\sim 35^{\circ}\text{N}$ and $93\sim 110^{\circ}\text{E}$); for the SEASM- the 5 highest (1990, 1997, 2000, 2001, and 2002) and the 5 lowest (1983, 1984, 1985, 1989, and 1995) years of MAM NDVI in Mongolia ($45\sim 58^{\circ}\text{N}$ and $80\sim 115^{\circ}\text{E}$), and the 5 highest (1990, 1994, 1998, 2001, and 2002) and the 5 lowest (1984, 1985, 1986, 1989, and 1996) years of MAM NDVI in western Asia ($32\sim 48^{\circ}\text{N}$ and $60\sim 80^{\circ}\text{E}$). Composite differences are calculated by subtracting the mean values for the 5 lowest years of MAM NDVI from the 5 highest years. To understand physically the relationship between the NEASM and spring vegetation activity in the surrounding lands (i.e., NA and SA regions), we use the composite analysis of soil moisture, LHF, SHF, and 2m temperature for the relationship between the NEASM and MAM NDVI in NA, and of soil moisture and 850 hPa wind vector for the NEASM and

MAM NDVI in SA. A Student's *t*-test for unequal population variance is conducted to quantify the statistical significance of the composite differences, and significant regions at the 90% level are contoured. Multivariate linear regression is applied to develop the forecast model for NEASM and SEASM rainfall [Lee *et al.*, 2008a]. Advanced statistical methods, i.e., generalized cross validation, colinearity diagnostic, and cross-validated estimation, have been performed in our study.

3. Relationships Between EASM Rainfall and Vegetation Activity

[10] The spatial distributions of EOF 1 of MAM NDVI anomalies show positive eigenvalues over the entire Asian continent with higher values in northern and southern Asia (Figure 1a). The time series of the corresponding standardized PC 1 for 1982~2003 show an increasing trend (Figure 1b). This result is consistent with the 1982~2003 regression trend of MAM NDVI, which shows significant increases in northern and southern Asia (Figure 1c). In order to determine the effects of vegetation activity in the surrounding lands on the EASM, we calculate correlation coefficients of area-averaged JJA rainfall over the sub-EASM regions with seasonally averaged NDVI in each grid over Asia.

3.1. NEASM Rainfall

[11] NDVI anomalies in the Tibetan Plateau (TP) during the preceding December through February (DJF) are significantly and negatively correlated with NEASM rainfall anomalies (Figure 2a). There is a significant positive correlation between NEASM rainfall and DJF NDVI in the island of Borneo in Southeast Asia (SEA). The area of each region is described in Table 1. NEASM rainfall anomalies are negatively correlated with the preceding MAM NDVI anomalies in central and northern Asia, and positively correlated with the preceding MAM NDVI anomalies in southern and northeastern Asia (NEA) (Figure 2b). Thus, increasing spring vegetation activity in NA and SA shown in Figure 1 is significantly related to NEASM rainfall with negative and positive correlations, respectively. We calculate the area-averaged MAM NDVI anomalies in NA (left box in Figure 2b) and SA (center box in Figure 2b), which are used in composite analysis to examine the 5 highest and lowest years of MAM NDVI in NA and SA. Correlation patterns during JJA (Figure 2c) are different from those during preceding MAM. Significant negative correlation in NA does not appear during JJA, and there is a positive correlation between JJA NDVI and NEASM rainfall anomalies. The negative signs of correlation coefficients in SA and northeastern Asia during JJA are also opposite of those during preceding MAM.

[12] The composite difference of JJA rainfall between the 5 years of highest and 5 years of lowest MAM NDVI in NA shows less rainfall in the NEASM region, especially the southern Japan, for the 5 highest years (Figure 3a). For the years of highest MAM NDVI in NA, there is weak upper-level divergence over the NEASM region (Figure 3b), which coincides with weak lower-level convergence. A significantly negative difference in upper-level divergence when subtracting the divergence of the 5 lowest years of MAM NDVI in NA from the 5 highest years occurs over the Korean peninsula and western North Pacific. The

Table 1. Areas and Correlation Values of Potential Predictors of NEASM and SEASM Rainfall^a

Response Variables	Potential Predictors	Areas	Correlation Values		
NEASM rainfall	Ocean factors	DJF SST in the TEP	5°S–5°N, 170°–80°W	+0.51*	
		DJF SST in the TWP ^b	0°–15°N, 130°–160°E	–0.47*	
		DJF SST in the TIO	10°S–10°N, 40°–100°E	+0.56**	
		DJF SST in the SSP	20°–35°S, 170°–140°W	–0.47*	
		DJF OHC in the TEP	10°S–5°N, 130°–90°W	+0.53*	
		DJF OHC in the TWP	10°S–5°N, 140°–180°E	–0.51*	
		DJF OHC in the TIO	20°S–15°N, 50°–70°E	+0.56**	
		MAM SST in the TEP	5°S–5°N, 170°–80°W	+0.44*	
		MAM SST in the TWP	0°–15°N, 130°–160°E	–0.45*	
		MAM SST in the TIO	10°S–10°N, 40°–100°E	+0.57**	
	MAM SST in the SSP	20°–40°S, 160°–120°W	–0.51*		
	MAM OHC in the TEP	15°S–0°, 130°–90°W	+0.46*		
	MAM OHC in the TWP	10°S–5°N, 140°–180°E	–0.45*		
	MAM OHC in the TIO	0°–20°S, 50°–70°E	+0.50*		
	Land factors	DJF NDVI in the TP	28°–45°N, 75°–100°E	–0.52*	
		DJF NDVI in the SEA	5°S–10°N, 95°–120°E	+0.57**	
		MAM NDVI in the NA	45°–60°N, 60°–90°E	–0.39	
		MAM NDVI in the NEA	40°–50°N, 120°–140°E	+0.39	
		MAM NDVI in the SA	20°–35°N, 93°–110°E	+0.68**	
		SEASM rainfall	Ocean factors	DJF SST in the ENP ^b	10°–25°N, 160°–120°W
DJF SST in the WNP				20°–30°N, 150°–180°E	+0.42*
DJF SST in the CPS ^b				0°–40°N, 110°–130°E	+0.40
DJF SST in the SSP				20°–35°S, 180°–140°W	+0.52*
DJF OHC in the WNP				10°–25°N, 160°E–165°W	+0.45*
DJF OHC in the SCS ^b	5°–20°N, 110°–130°E			+0.55**	
DJF OHC in the SSP	10°–25°S, 155°E–165°W			+0.45*	
MAM SST in the ENP	10°–25°N, 160°–120°W			–0.49*	
MAM SST in the CPS	0°–40°N, 110°–130°E			+0.51*	
MAM SST in the SSP	20°–35°S, 180°–140°W			+0.43*	
MAM OHC in the WNP	20°–30°N, 140°E–150°W	+0.53*			
MAM OHC in the SCS	5°–20°N, 110°–130°E	+0.32			
MAM OHC in the TIO	5°S–5°N, 50°–80°E	+0.61**			
MAM OHC in the SIO	10°–20°S, 70°–100°E	–0.35			
MAM OHC in the SEIO ^b	5°–30°S, 100°–120°E	+0.57**			
MAM OHC in the SSP	10°–25°S, 155°–165°W	+0.46*			
Land factors	DJF NDVI in the ICP	10°–33°N, 92°–110°E	–0.37		
	MAM NDVI in MO	45°–58°N, 80°–115°E	+0.48*		
	MAM NDVI in the WA	32°–48°N, 60°–80°E	+0.49*		

^aBold represents the selected predictors. Here ** and * represent that correlations are significant at $\alpha = 0.01$ and 0.05 levels, respectively.

^bTWP, tropical western Pacific; ENP, eastern North Pacific; CPS, East and South China and Philippine Seas; SCS, South China Sea; SEIO, southeastern Indian Ocean.

weakened (or enhanced) NEASM for the years of highest (or lowest) MAM NDVI in NA is consistent with a significant negative correlation between NEASM rainfall and the preceding MAM NDVI anomalies in NA shown in Figure 2b. Figures 3c and 3d show the composite differences of JJA rainfall and JJA 150 hPa divergence between the 5 years of highest and of lowest MAM NDVI in SA. There is more (or less) JJA rainfall and stronger (or weaker) JJA upper-level divergence over the NEASM region for the years of highest (or lowest) MAM NDVI in SA. Significantly positive differences in rainfall and upper-level divergence are in the regional frontal zones of the NEASM: the Mei-yu in eastern China, Changma in Korea, and Baiu in Japan. Again, the stronger (or weaker) NEASM for the years of highest (or lowest) MAM NDVI in SA is consistent with a significant positive correlation between NEASM rainfall and the preceding MAM NDVI anomalies in SA shown in Figure 2b.

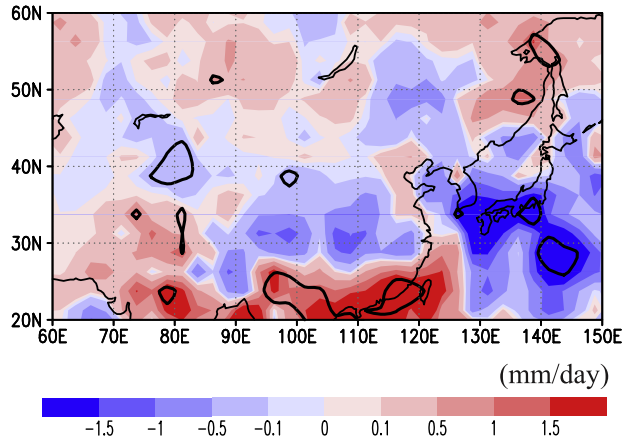
3.2. SEASM Rainfall

[13] SEASM rainfall anomalies are significantly and negatively correlated with the preceding DJF NDVI anomalies in the Indochina peninsula (ICP) (Figure 2d). They are

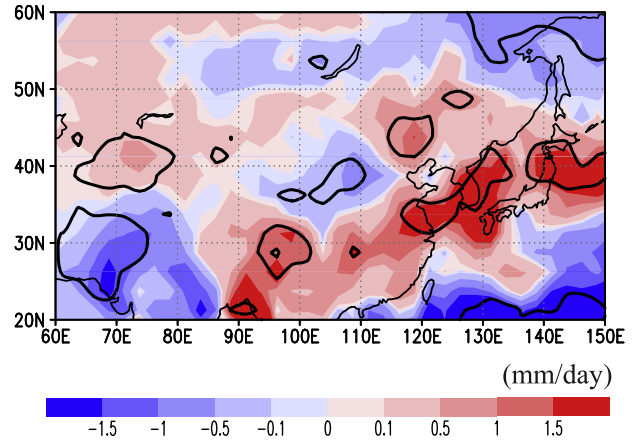
positively correlated with the preceding MAM NDVI anomalies in Mongolia (MO) and western Asia (WA) (Figure 2e). Thus, increasing spring vegetation activity in northern Asia shown in Figure 1 is also significantly related to SEASM rainfall with a positive correlation. We calculate the area-averaged MAM NDVI anomalies in MO (upper box in Figure 2e) and WA (lower box in Figure 2e), which are used in composite analysis to examine the 5 highest and lowest years of MAM NDVI in MO and WA. During JJA, there are significant positive correlation in TP and negative correlation in the southeastern China and ICP.

[14] Figures 4a and 4b show the composite differences of JJA rainfall and JJA 150 hPa divergence between the 5 years of highest and of lowest MAM NDVI in MO. There are more (or less) JJA rainfall and stronger (or weaker) JJA upper-level divergence over the SEASM region, especially the southeastern China, for the years of highest (or lowest) MAM NDVI in MO. The enhanced (or weakened) SEASM for the years of highest (or lowest) MAM NDVI in MO is consistent with a significant positive correlation between SEASM rainfall and the preceding MAM NDVI anomalies in MO shown in Figure 2e. For the 5 years of highest (or

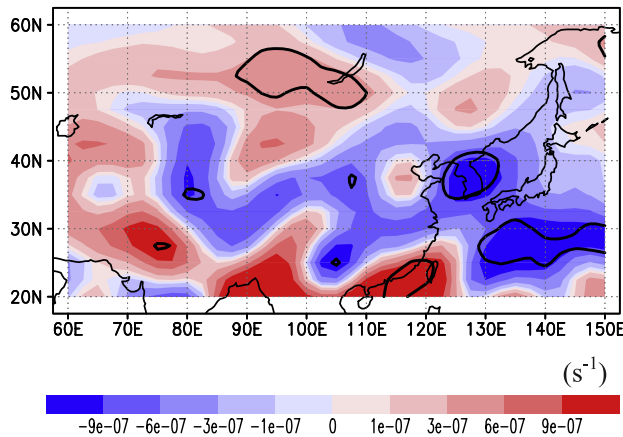
(a) JJA rainfall composite for NA



(c) JJA rainfall composite for SA



(b) JJA 150 hPa divergence composite for NA



(d) JJA 150 hPa divergence composite for SA

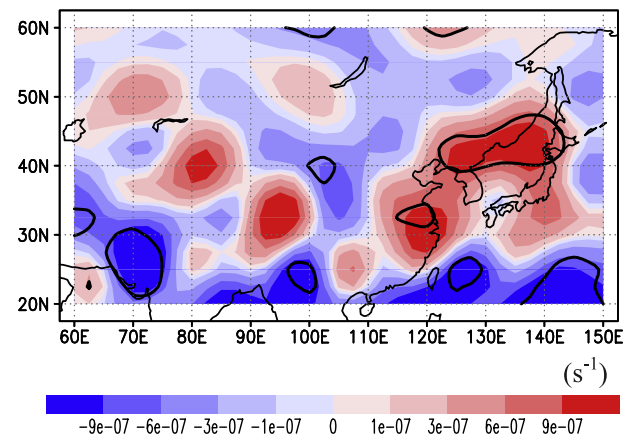


Figure 3. Composite differences of (a) JJA rainfall (mm/d) and (b) JJA 150 hPa divergence (s^{-1}) for the 5 years of highest and of lowest MAM NDVI in NA, and (c) JJA rainfall and (d) JJA 150 hPa divergence for the 5 years of highest and of lowest MAM NDVI in SA. Positive (red) and negative (blue) values represent divergences and convergences in Figures 3b and 3d. Significant regions at the 90% are contoured.

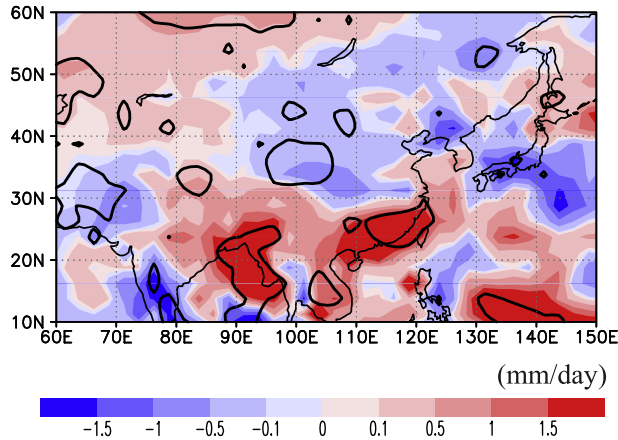
lowest) MAM NDVI in WA, the composite differences of JJA rainfall (Figure 4c) and 150 hPa divergence (Figure 4d) between the 5 years of highest and of lowest MAM NDVI in WA show more (or less) rainfall and stronger (or weaker) upper-level divergence in the SEASM region. Again, the stronger (or weaker) SEASM for the years of highest (or lowest) MAM NDVI in WA is consistent with a significant positive correlation between SEASM rainfall and the preceding MAM NDVI anomalies in WA shown in Figure 2e.

4. Physical Mechanisms Between the NEASM and MAM NDVI

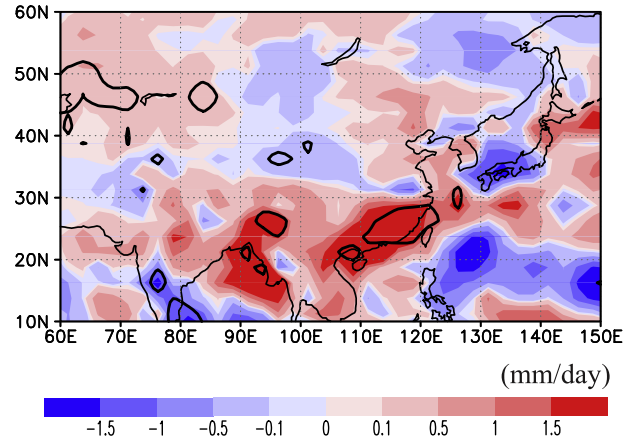
[15] The composite difference of MAMJJA LHF between the 5 years of highest and of lowest MAM NDVI is positive over NA (Figure 5a). A positive difference in the LHF is consistent with a negative composite difference in the MAM SHF over the same region (Figure 5b). Increased LHF and decreased SHF due to increased MAM NDVI has been observed in the Indian summer monsoon region [Lee

et al., 2008b], consistent with our results. A positive LHF and negative SHF over NA in the composite differences result in a negative JJA 2m temperature over the same region in the composite difference between the 5 years of highest and of lowest MAM NDVI (Figure 5c). This result is consistent with previous modeling [e.g., Xue, 1997] and observational [Lee *et al.*, 2008b] studies. JJA 2m temperature in NA is different from that in the northwestern Pacific; negative over NA and positive over the adjacent oceans for the years of highest MAM NDVI in NA. These differences in surface air temperature can cause a decrease in heat contrast between land and sea, which plays an important role in controlling the monsoon [e.g., Meehl, 1994]. For the years of highest (or lowest) MAM NDVI in NA, there are fewer (or more) cyclonic anomalies in the NEASM region, which create a weaker (or stronger) NEASM (Figure 5c). Thus, the significant negative correlation between NEASM rainfall and the preceding MAM NDVI anomalies in NA (Figure 2b) appears related to the weakened (or enhanced) land-sea heat contrast, which is a result of the increase (or

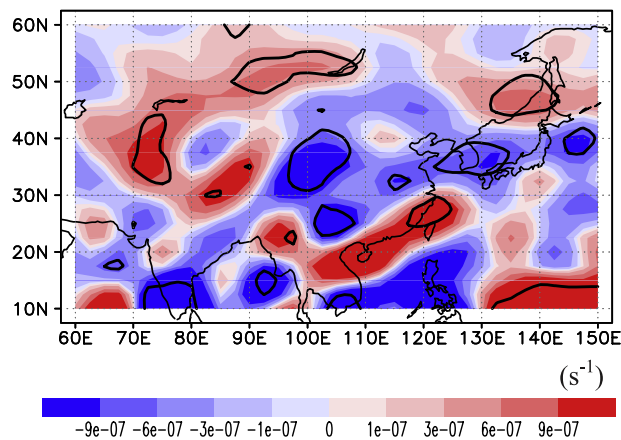
(a) JJA rainfall composite for MO



(c) JJA rainfall composite for WA



(b) JJA 150 hPa divergence composite for MO



(d) JJA 150 hPa divergence composite for WA

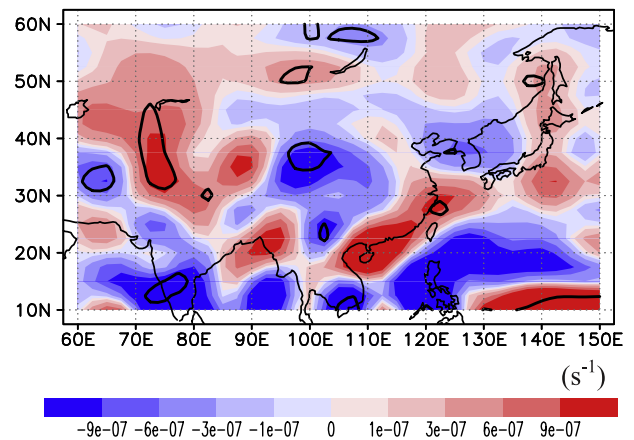


Figure 4. As in Figure 3, but with composite differences for MAM NDVI in (a) and (b) MO, and for MAM NDVI in (c) and (d) WA.

decrease) in spring vegetation related to increased (or decreased) early spring soil moisture (Figure 5d), both of which would act to favor an increase (or decrease) in LHF (Figure 5a) and a decrease (or increase) in SHF (Figure 5b). This result is consistent with the physical relationship between spring vegetation activity and early Indian summer monsoon rainfall [Lee *et al.*, 2008b].

[16] For the physical mechanism between the NEASM and spring vegetation activity in SA, we use the composite analysis of soil moisture between 0 and 10 cm BGL and 850 hPa wind vector between the 5 years of highest and of lowest MAM NDVI in SA. There is a significantly positive difference in spring soil moisture in southern and eastern China when subtracting the soil moisture of the 5 lowest years of MAM NDVI in SA from the 5 highest years (Figure 5e). The increased (or decreased) soil moisture provides an increased (or decreased) atmospheric moisture source, which affects NEASM rainfall through the climatological southwesterly wind flowing into the NEASM region and which is stronger (or weaker) for the years of highest (or lowest) MAM NDVI in SA (Figure 5e). This increased (or decreased) atmospheric moisture is also related to an intensified (or weakened) southwesterly wind due to stron-

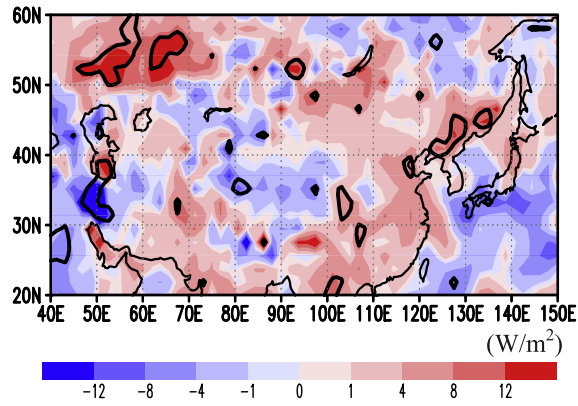
ger (or weaker) cyclonic anomalies in the NEASM region and stronger (or weaker) anticyclonic anomalies in the western North Pacific, which serves to advect more (or less) moisture from the wet (or dry) soils, for the years of highest (or lowest) MAM NDVI in SA. It is possible that the stronger (or weaker) anticyclonic circulation in the western North Pacific also advects more (or less) moisture from the western North Pacific. Thus, the significant positive correlation between NEASM rainfall and the preceding MAM NDVI anomalies in SA (Figure 2b) appears related to the increased (or decreased) moisture by more (or less) evapotranspiration due to increase (or decrease) in spring vegetation activity, which flows into the NEASM region through the increased (or decreased) southwesterly airflow.

5. Improved Forecast Models for NEASM and SEASM Rainfall

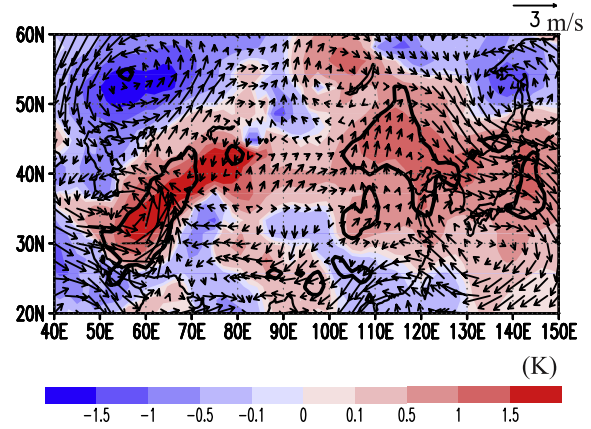
5.1. Forecast Models

[17] Land cover indices in the surrounding lands defined by the spatial correlation analysis between EASM rainfall and NDVI anomalies during the previous spring (MAM) and winter (DJF), which is defined as the premonsoon

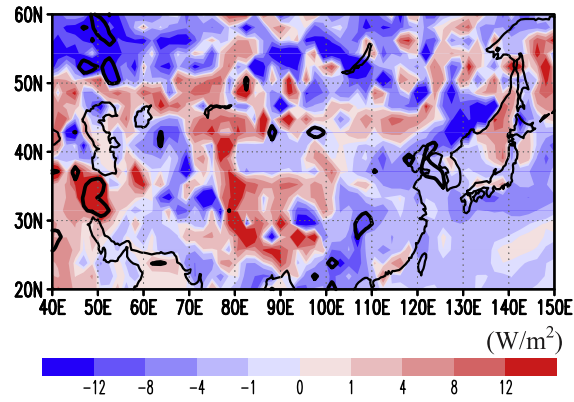
(a) MAMJJA LHF composite for NA



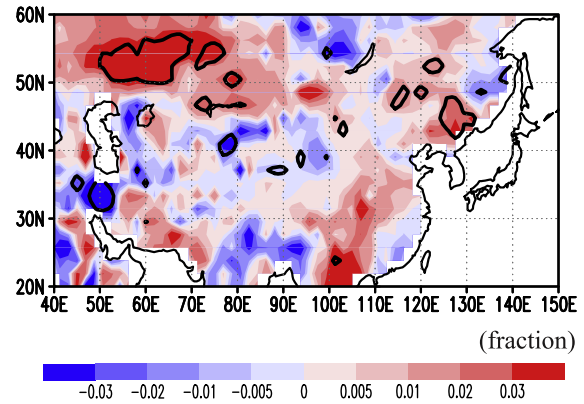
(c) JJA 2m temp and 850 hPa wind composites for NA



(b) MAM SHF composite for NA



(d) March soil moisture composite for NA



(e) MAM soil moisture and JJA 850 hPa wind composites for SA

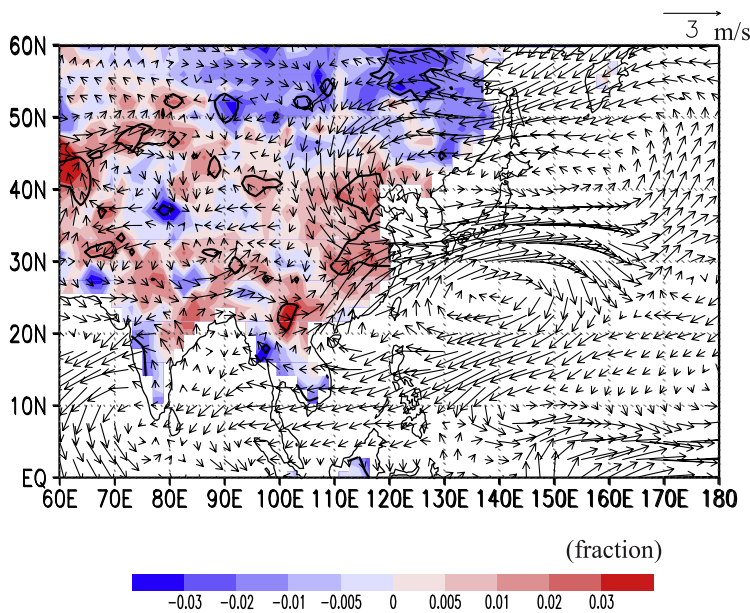


Figure 5

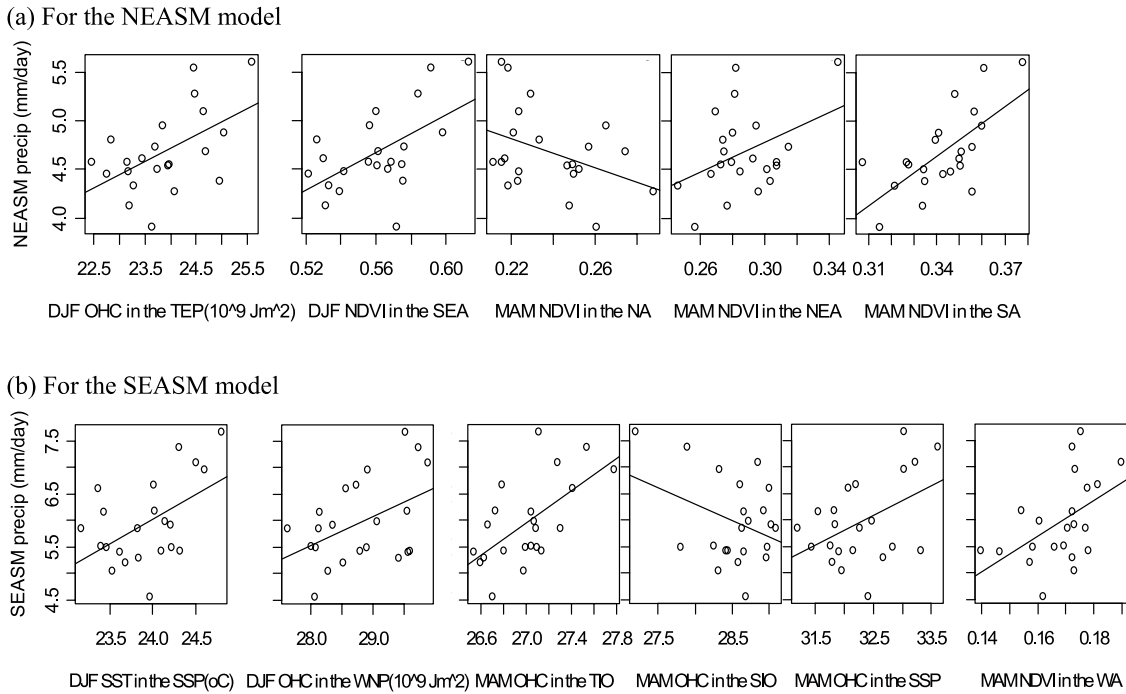


Figure 6. Scatterplots of (a) NEASM rainfall and its selected predictors, i.e., DJF OHC in the TEP ($r = +0.53$), DJF NDVI in the SEA ($r = +0.57$), MAM NDVI in the NA ($r = -0.39$), MAM NDVI in the NEA ($r = +0.39$) and MAM NDVI in the SA ($r = +0.68$), and (b) SEASM rainfall and its selected predictor, i.e., DJF SST in the SSP ($r = +0.52$), DJF OHC in the WNP ($r = +0.45$), MAM OHC in the TIO ($r = +0.61$), MAM OHC in the SIO ($r = -0.35$), MAM OHC in the SSP ($r = +0.46$) and MAM NDVI in the WA ($r = +0.49$).

season, are included to enhance the predictive skill of the EASM forecast models performed by only oceanic heat sources [Lee et al., 2008a]. Using the Mallows C_p , predicted residual sums of squares ($PRESS$) and F -statistic methods [e.g., Helsel and Hirsch, 1992], which give the same selection of predictors, DJF OHC in the tropical eastern Pacific (TEP) as an ocean factor, and DJF NDVI in the SEA, MAM NDVI in the NA, MAM NDVI in the NEA and MAM NDVI in the SA as land factors are selected for NEASM rainfall (indicated in bold in Table 1). For SEASM rainfall, the generalized cross validation (GCV) score is additionally computed, because C_p and $PRESS$ give different combinations of predictors as the best subset. The GCV function is a good estimate of predictive error of the model, unlike other functions which are goodness of fit measures [Craven and Whaba, 1978]. For a range of values of neighborhood size (K) and polynomial order (p), the combination that provides the minimum GCV value is selected [Grantz et al., 2005].

[18] The GCV (K, p) score function is defined as

$$GCV(K, p) = \frac{\sum_{i=1}^n \frac{e_i^2}{N}}{(1 - \frac{m}{N})^2} \quad (2)$$

where e^i is the error, N is the number of data points, and m is the number of parameters [Grantz et al., 2005].

[19] Both $PRESS$ and GCV statistics select the same selection of predictors for SEASM rainfall, which are DJF SST in the subtropical South Pacific (SSP), DJF OHC in the western North Pacific (WNP), MAM OHC in the tropical Indian Ocean (TIO), MAM OHC in the southern Indian Ocean (SIO) and MAM OHC in the SSP as ocean factors, and MAM NDVI in the WA as a land factor are selected; these are also indicated in bold in Table 1. Figure 6 shows scatterplots of NEASM and SEASM rainfall and the selected predictors.

[20] In the detrended regression model for NEASM rainfall (equation (4)), MAM NDVIs in NA and SA are selected as significant predictors, which are physically related to the NEASM and explained in section 4. As other selected predictors, there are DJF NDVI in the SEA, MAM NDVI in the NEA, and DJF OHC in the TEP. The relative importance of the predictors to the overall model is ordered by MAM NDVI in the SA (0.84), DJF NDVI in the SEA (0.71), MAM NDVI in the NA (-0.69), MAM NDVI in the NEA (-0.54), and DJF OHC in the TEP (-0.50) in terms of the partial correlations in parentheses. The predictors are correlated among themselves (i.e., multicollinearity), so collinearity diagnostics using variance inflation factor

Figure 5. Composite differences of (a) MAMJJA LHF (W/m^2), (b) MAM SHF (W/m^2), (c) JJA 2m temperature (K) and JJA 850 hPa wind vector (m/s), and (d) March soil moisture between 0 and 10 cm BGL (fraction) for the 5 years of highest and of lowest MAM NDVI in NA, and (e) MAM soil moisture between 0 and 10 cm BGL (fraction) and JJA 850 hPa wind vector (m/s) for the 5 years of highest and of lowest MAM NDVI in SA. Significant regions at the 90% are contoured.

(VIF) have been performed. The VIF is the reciprocal of the amount of variance in an independent variable that is not explained by the other independent variables (i.e., tolerance; $1-r_k^2$) [Rogerson, 2001].

[21] Specifically,

$$\text{VIF}_k = \frac{1}{1-r_k^2} \quad k = 1, 2, \dots, p-1 \quad (3)$$

where r_k^2 is the coefficient of multiple determination when X_k is regressed on the $p-2$ other X variables in the model [Neter et al., 1996].

[22] If the VIF is greater than about 5 [Rogerson, 2001] or 10 [Neter et al., 1996], this indicates potential multicollinearity problems. The VIFs of all selected predictors for the NEASM model are lower than 5 indicating there are no multicollinearity problems (VIF values- DJF OHC in the TEP: 4.1, DJF NDVI in the SEA: 3.5, MAM NDVI in the NA: 1.1, MAM NDVI in the NEA: 1.9, and MAM NDVI in the SA: 2.4). The goodness of fit in the overall model shows a significant p -value at significance level (α) = 0.01 in terms of F -statistic; also, p -values of t -statistics of all independent variables are significant at $\alpha = 0.05$. The correlation and R^2 for the NEASM rainfall model are 0.92 and 0.85. Adjusted R^2 is 0.80, thus 80% of the variance of NEASM rainfall can be explained by the selected predictors in the model. The forecast model including land cover indices doubles the predictive skill over that using only oceanic heat sources, which is 42% [Lee et al., 2008a].

$$\begin{aligned} \text{NEASM rainfall} = & -1.51 - 0.23 \text{ DJF OHC in the TEP} \\ & + 12.76 \text{ DJF NDVI in the SEA} \\ & - 7.56 \text{ MAM NDVI in the NA} \\ & - 6.81 \text{ MAM NDVI in the NEA} \\ & + 24.29 \text{ MAM NDVI in the SA} \end{aligned} \quad (4)$$

The linear regression model for SEASM rainfall (equation (5)) has six predictors, five predictors are ocean factors and one is a land factor. The relative importance of the predictors to the overall model is ordered by MAM OHC in the TIO (0.83), DJF OHC in the WNP (0.80), MAM NDVI in the WA (0.75), MAM OHC in the SSP (-0.67), MAM OHC in the SIO (-0.52), and DJF SST in the SSP (0.51) in terms of the partial correlations. The VIFs of all selected predictors for the SEASM model are lower than 5 indicating there are no multicollinearity problems (VIF values- DJF SST in the SSP: 3.3, DJF OHC in the WNP: 2.4, MAM OHC in the TIO: 1.2, MAM OHC in the SIO: 1.5, MAM OHC in the SSP: 3.9, and MAM NDVI in the WA: 1.4). The overall goodness of fit is statistically significant with the correlation of 0.92 and R^2 of 0.85. Adjusted R^2 is 0.79, thus the forecast model including land cover and OHC factors triples the predictive skill over that using only SST, which is 24% [Lee et al., 2008a].

$$\begin{aligned} \text{SEASM rainfall} = & -37.21 + 0.77 \text{ DJF SST in the SSP} \\ & + 0.98 \text{ DJF OHC in the WNP} \\ & + 1.54 \text{ MAM OHC in the TIO} \\ & - 0.51 \text{ MAM OHC in the SIO} \\ & - 1.15 \text{ MAM OHC in the SSP} \\ & + 41.19 \text{ MAM NDVI in the WA} \end{aligned} \quad (5)$$

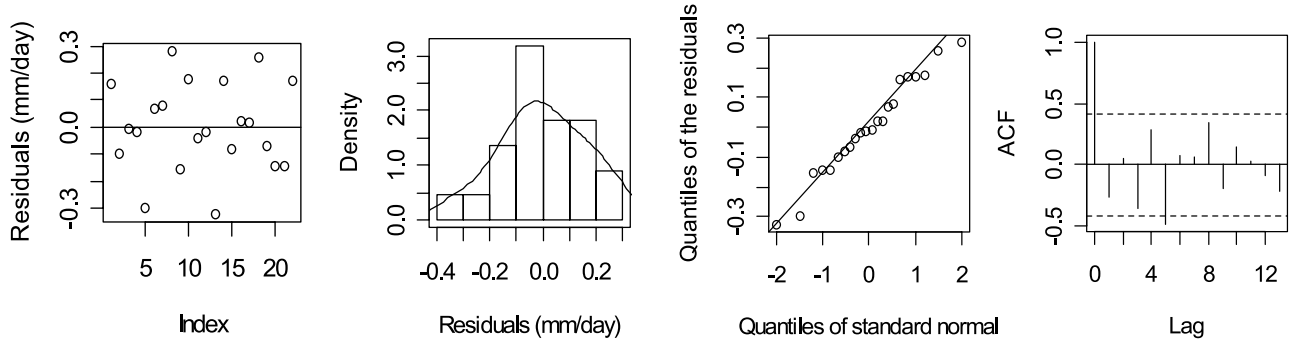
5.2. Model Results and Diagnostics

[23] Key assumptions of linear regression are that the random errors are independent, identically distributed with mean zero and common variance [Walpole et al., 2002]. The scatterplots, histogram and quantile-quantile (Q-Q) plot of the residuals of the NEASM (Figure 7a) and SEASM (Figure 7b) models suggest that they are normally distributed with a mean of zero. The scatterplots of the residuals (left panels) suggest the means of residuals are very close to zero by evenly distributed residuals around the lines. Histograms and probability density functions of residuals (center left panels) show that the residuals appear normally distributed with a mean around zero. In Q-Q plots (center right panels), the quantiles of the residuals show good fit with the quantiles of standard normal. The assumption of normal distribution for the residuals is also confirmed by one-sample Kolmogorov-Smirnov (KS) test [von Storch and Zwiers, 2001] failing to reject the null hypothesis that expected empirical cumulative distribution function (CDF) of the residuals is not different with observed CDF of the residuals (p -values are 0.94 for the NEASM and 0.97 for the SEASM models). Autocorrelation function (ACF) plots of the residuals (right panels in Figures 7a and 7b) denote that there are no significant serial autocorrelations, because if no ACF estimates fall outside the 95% confidence limit (shown as the dotted lines in ACF figures), one can safely assume there is no autocorrelation [Neumann et al., 2003]. The ACF plot in Figure 7a shows that there is some autocorrelation between the residuals at lag 5, but the rest are well below the significant line- indicating they are statistically insignificant. Thus, model results by statistical inspections show the normality and independence of the residuals.

[24] In order to check the predictive capability of the models, a cross-validated estimation is performed [e.g., Grantz et al., 2005]. In this analysis, the observations for a year are dropped and the model is fitted using the remaining observations. The fitted model is then used to estimate (predict) the rainfall value for the dropped year; this is repeated for all the years [Neumann et al., 2003]. The cross-validated estimates and the observed rainfall for the NEASM and SEASM are shown in Figures 8 and 9, which show very good agreements between the estimated values and their observed rainfall in comparison to Figures 8 and 9 in Lee et al. [2008a]. The R^2 values of the cross-validated estimates and the observed are same for NEASM and SEASM rainfall (0.71). They show highly improved predictive skill in comparison to those of the models using only ocean factors, which are 0.21 and 0.16 for NEASM and SEASM rainfall, respectively [Lee et al., 2008a].

[25] As a robust check, we drop 10% of the points and again fit the model that is used to estimate the rainfall value for the dropped years; this is repeated 250 times with randomly dropping points. The root mean square (RMS) errors of the dropped predictions for the NEASM and SEASM rainfall models are 0.17 and 0.31 mm/d, which are within 5% of the mean rainfall (mean NEASM and SEASM rainfall are 4.61 and 5.41 mm/d with variances of 0.18 and 0.55 mm/d, respectively). The RMS errors for the NEASM and SEASM rainfall models are 0.16 and 0.28 mm/d, which are also within 5% of the mean rainfall. They are smaller than those from the models using only ocean factors, which are 0.27 and 0.63 mm/d for NEASM

(a) For the NEASM model



(b) For the SEASM model

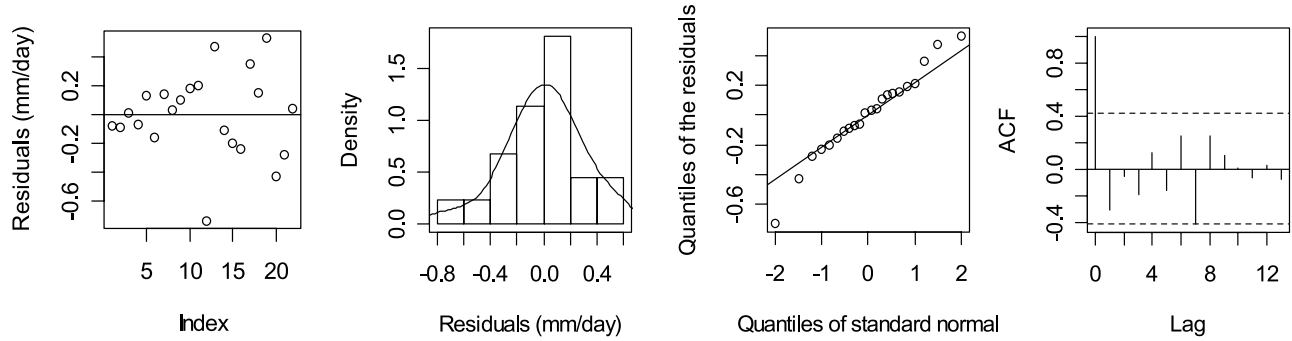


Figure 7. Tests for the normality and autocorrelation of the residuals for the (a) NEASM rainfall and (b) SEASM rainfall models. The dotted lines in the figures of autocorrelation function (ACF) represent the 95% confidence lines.

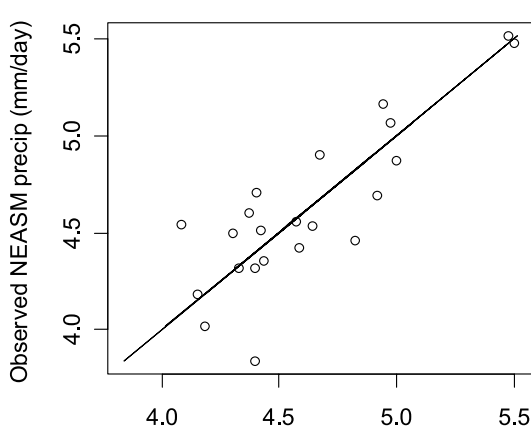
and SEASM rainfall models [Lee et al., 2008a]. We note that regressions are often not stationary with time and the diagnostics we have performed here are no guarantee of stationarity. Therefore, these relationships will have to be constantly monitored [e.g., Kumar et al., 1999].

6. Conclusions

[26] Forecasting models for NEASM and SEASM rainfall using a combination of the surrounding factors in the lands

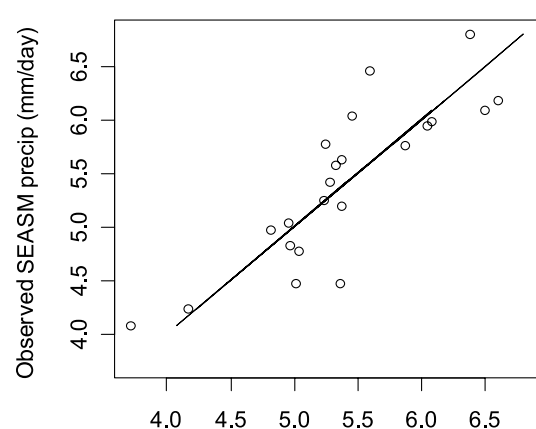
and oceans greatly increased monsoon predictive skill and shows that the condition of the premonsoon land surface is an important factor in the formation of monsoon precipitation. Of course the condition of the land surface is partially a function of previous weather conditions with the land surface providing memory of these conditions. This study identified statistical and physical relationships between the EASM and spring vegetation activity in the surrounding lands. In this analysis we find the following.

(a)



Cross validation estimated NEASM precip (mm/day)

(b)



Cross validation estimated SEASM precip (mm/day)

Figure 8. Scatterplots of cross-validated and observed values for (a) NEASM rainfall and (b) SEASM rainfall.

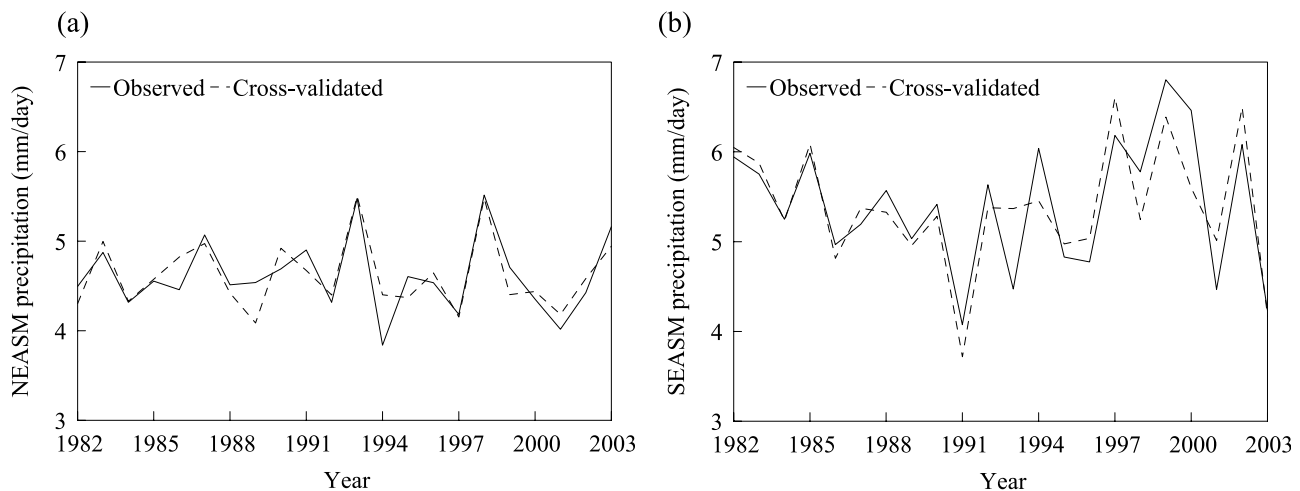


Figure 9. Comparisons of cross-validated values (dotted lines) with observed values (solid lines) for (a) NEASM rainfall and (b) SEASM rainfall.

[27] 1. 80% and 79% of NEASM and SEASM rainfall variances can be explained by a combination of land cover and ocean indices during the premonsoon season. This can be compared with 42% and 24% when only oceanic heat sources are included.

[28] 2. NDVI increased significantly from 1982~2003 during the premonsoon season (MAM) over the Asian continent with very strong increases in northern and southern Asia.

[29] 3. NEASM rainfall anomalies have significant correlations with premonsoon NDVI anomalies in the Asian continent, which are negative in central and northern Asia and positive in southern Asia. SEASM rainfall anomalies have significant positive correlations with MAM NDVI anomalies in Mongolia and western Asia.

[30] 4. Composite analysis of rainfall and upper-level divergence shows that the NEASM is weaker (or stronger) for the years having more (or less) spring vegetation activity in northern Asia, and is stronger (or weaker) for the years having more (or less) spring vegetation activity in southern Asia. Composite analysis for the SEASM shows the SEASM is stronger (or weaker) for the years having more (or less) spring vegetation in Mongolia and western Asia.

[31] 5. We infer physical mechanisms based on incomplete observational data. A weaker NEASM is brought about by the weakened land-sea heat contrast, which is a result of the increase in spring vegetation activity in northern Asia related to increased soil moisture. A stronger NEASM is affected by the enhanced southwesterly airflow having more moisture due to increased spring vegetation activity in southern Asia.

[32] The physical mechanisms between the SEASM and the premonsoon land surface conditions need to be investigated further. Whether the land conditions are the actual cause of the monsoon effects the next summer, or simply serve as a proxy for variations in the atmospheric flow patterns is not clear yet. Firmly establishing the vegetation-rainfall connection will require more detailed future measurements calculated from observational data sets combined with general circulation model simulations, which hopefully will become available in the future [Lee et al., 2008b].

[33] **Acknowledgments.** We acknowledge for providing the data sets; the Global Land Cover Facility for NDVI, the World Climate Research Program Global Energy and Water Cycle Experiment project for GPCP precipitation, the National Centers for Environmental Prediction and Department of Energy for the reanalysis data, the Met Office Hadley Centre for Climate Prediction and Research for SST, and the Scripps Institution of Oceanography for OHC. We wish to thank the anonymous reviewers for valuable suggestions. Partial support of this work by National Science Foundation via grant ATM-0437538 is also thankfully acknowledged. Eungul Lee was partially supported by the Gilbert F. White Doctoral Fellowship in the Department of Geography at the University of Colorado.

References

- Adler, R. F., et al. (2003), The version-2 global precipitation climatology project (GPCP) monthly precipitation analysis (1979–present), *J. Hydrometeorol.*, *4*, 1147–1167, doi:10.1175/1525-7541(2003)004<1147:TVGPCP>2.0.CO;2.
- Biggs, T. W., P. S. Thenkabail, M. K. Gumma, C. Scott, G. R. Parthasaradhi, and H. Tural (2006), Irrigated area mapping in heterogeneous landscapes with MODIS time series, ground truth and census data, Krishna Basin, India, *Int. J. Remote Sens.*, *27*, 4245–4266, doi:10.1080/01431160600851801.
- Chang, C.-P., Y. Zhang, and T. Li (2000), Interannual and interdecadal variations of the East Asian summer monsoon and tropical Pacific SSTs. Part I: Roles of the subtropical ridge, *J. Clim.*, *13*, 4310–4325, doi:10.1175/1520-0442(2000)013<4310:IAIVOT>2.0.CO;2.
- Cracknell, A. P. (1997), *The Advanced Very High Resolution Radiometer*, Taylor and Francis, London.
- Craven, P., and G. Whaba (1978), Optimal smoothing of noisy data with spline functions, *Numer. Math.*, *31*, 377–403, doi:10.1007/BF01404567.
- Defries, R. S., and A. S. Belward (2000), Global and regional land cover characterization from satellite data, *Int. J. Remote Sens.*, *21*, 1083–1092, doi:10.1080/014311600210083.
- D'Souza, G., A. S. Belward, and J. P. Malingreau (1996), *Advances in the Use of NOAA AVHRR Data for Land Applications*, Kluwer Acad., Dordrecht, Netherlands.
- Fu, C. (2003), Potential impacts of human-induced land cover change on East Asia monsoon, *Global Planet. Change*, *37*, 219–229.
- Grantz, K., B. Rajagopalan, M. Clark, and E. Zagana (2005), A technique for incorporating large-scale climate information in basin-scale ensemble streamflow forecasts, *Water Resour. Res.*, *41*, W10410, doi:10.1029/2004WR003467.
- Helsel, D. R., and R. M. Hirsch (1992), *Statistical Methods in Water Resources*, Elsevier Sci., Amsterdam.
- Kalnay, E., et al. (1996), The NCEP/NCAR 40-year reanalysis project, *Bull. Am. Meteorol. Soc.*, *77*, 437–471, doi:10.1175/1520-0477(1996)077<0437:TNYRP>2.0.CO;2.
- Kanamitsu, M., W. Ebisuzaki, J. Woollen, S.-K. Yang, J. J. Hnilo, M. Fiorino, and G. L. Potter (2002), NCEP-DOE AMIP-II reanalysis (R-2), *Bull. Am. Meteorol. Soc.*, *83*, 1631–1643, doi:10.1175/BAMS-83-11-1631(2002)083<1631:NAR>2.3.CO;2.

- Kumar, K. K., B. Rajagopalan, and M. A. Cane (1999), On the weakening relationship between the Indian monsoon and ENSO, *Science*, *284*, 2156–2159, doi:10.1126/science.284.5423.2156.
- Leavitt, S. W., T. N. Chase, B. Rajagopalan, E. Lee, and P. J. Lawrence (2008), Southwestern U.S. tree-ring carbon isotope indices as a possible proxy for reconstruction of greenness of vegetation, *Geophys. Res. Lett.*, *35*, L12704, doi:10.1029/2008GL033894.
- Lee, E.-J., J.-G. Jhun, and C.-K. Park (2005), Remote connection of the northeast Asian summer rainfall variation revealed by a newly defined monsoon index, *J. Clim.*, *18*, 4381–4393, doi:10.1175/JCLI3545.1.
- Lee, E., T. N. Chase, and B. Rajagopalan (2008a), Seasonal forecasting of East Asian summer monsoon based on oceanic heat sources, *Int. J. Climatol.*, *28*, 667–678, doi:10.1002/joc.1551.
- Lee, E., T. N. Chase, B. Rajagopalan, R. G. Barry, T. W. Biggs, and P. J. Lawrence (2008b), Effects of irrigation and vegetation activity on early Indian summer monsoon variability, *Int. J. Climatol.*, in press.
- Li, H., A. Robock, S. Liu, X. Mo, and P. Viterbo (2005), Evaluation of reanalysis soil moisture simulations using updated Chinese soil moisture observations, *J. Hydrometeorol.*, *6*, 180–193, doi:10.1175/JHM416.1.
- Meehl, G. A. (1994), Influence of the land surface in the Asian summer monsoon: External conditions versus internal feedback, *J. Clim.*, *7*, 1033–1049, doi:10.1175/1520-0442(1994)007<1033:TOTLSI>2.0.CO;2.
- Myneni, R. B., F. G. Hall, P. J. Sellers, and A. L. Marshak (1995), The interpretation of spectral vegetation indexes, *IEEE Trans. Geosci. Remote Sens.*, *33*, 481–486, doi:10.1109/36.377948.
- Neter, J., M. H. Kutner, C. J. Nachtsheim, and W. Wasserman (1996), *Applied Linear Statistical Models*, 4th ed., pp. 385–388, Irwin, Chicago.
- Neumann, D. W., B. Rajagopalan, and E. A. Zagona (2003), Regression model for daily maximum stream temperature, *J. Environ. Eng.*, *129*, 667–674, doi:10.1061/(ASCE)0733-9372(2003)129:7(667).
- Rayner, N. A., D. E. Parker, E. B. Horton, C. K. Folland, L. V. Alexander, D. P. Rowell, E. C. Kent, and A. Kaplan (2003), Global analyses of sea surface temperature, sea ice, and night marine air temperature since the late nineteenth century, *J. Geophys. Res.*, *108*(D14), 4407, doi:10.1029/2002JD002670.
- Rogerson, P. A. (2001), *Statistical Methods for Geography*, 136 pp., Sage, London.
- Sen, O. L., Y. Wang, and B. Wang (2004), Impact of Indochina deforestation on the East Asian summer monsoon, *J. Clim.*, *17*, 1366–1380, doi:10.1175/1520-0442(2004)017<1366:IOIDOT>2.0.CO;2.
- Tao, S. Y., and L. X. Chen (1987), A review of recent research on the East Asian summer monsoon in China, in *Monsoon Meteorology*, edited by C. P. Chang and T. N. Krishnamurti, pp. 60–92, Oxford Univ. Press, New York.
- Tomita, T., H. Sato, M. Nonaka, and M. Hara (2007), Interdecadal variability of the early summer surface heat flux in the Kuroshio region and its impact on the Baiu frontal activity, *Geophys. Res. Lett.*, *34*, L10708, doi:10.1029/2007GL029676.
- Townshend, J. R. G. (1994), Global data sets for land applications from the advanced very high resolution radiometer: An introduction, *Int. J. Remote Sens.*, *15*, 3319–3332, doi:10.1080/01431169408954333.
- Tucker, C. J., J. E. Pinzon, M. E. Brown, D. A. Slayback, E. W. Pak, R. Mahoney, E. F. Vermote, and N. Saleous (2005), An extended AVHRR 8-km NDVI dataset compatible with MODIS and SPOT vegetation NDVI data, *Int. J. Remote Sens.*, *26*, 4485–4498, doi:10.1080/01431160500168686.
- von Storch, H., and F. W. Zwiers (2001), *Statistical Analysis in Climate Research*, Cambridge Univ. Press, Cambridge, UK.
- Walpole, R. E., R. H. Myers, S. L. Myers, and K. Ye (2002), *Probability and Statistics for Engineers and Scientists*, 7th ed., 402 pp., Prentice-Hall, Upper Saddle River, N. J.
- Wang, B., and T. Li (2004), East Asian monsoon-ENSO interactions, in *East Asian Monsoon*, edited by C.-P. Chang, pp. 177–212, World Sci., Singapore.
- Webster, P. J. (1987), The elementary monsoon, in *Monsoons*, edited by J. S. Fein and P. L. Stephens, pp. 3–32, John Wiley, New York.
- White, W. B., D. R. Cayan, M. D. Dettinger, and G. Auad (2001), Sources of global warming in upper ocean temperature during El Niño, *J. Geophys. Res.*, *106*, 4349–4367, doi:10.1029/1999JC000130.
- Wu, R., and B. Wang (2002), A contrast of the East Asian summer monsoon-ENSO relationship between 1962–77 and 1978–93, *J. Clim.*, *15*, 3266–3279, doi:10.1175/1520-0442(2002)015<3266:ACOTEA>2.0.CO;2.
- Xue, Y. (1996), The impact of desertification in the Mongolian and inner-Mongolian grassland on the regional climate, *J. Clim.*, *9*, 2173–2189, doi:10.1175/1520-0442(1996)009<2173:TIODIT>2.0.CO;2.
- Xue, Y. (1997), Biosphere feedback on regional climate in tropical north Africa, *Q. J. R. Meteorol. Soc.*, *123*, 1483–1515, doi:10.1002/qj.49712354203.
- Yihui, D. (1994), *Monsoons Over China*, Kluwer Acad., Dordrecht, Netherlands.

T. N. Chase and B. Rajagopalan, Cooperative Institute for Research in Environmental Sciences, University of Colorado, Boulder, CO 80309, USA.

E. Lee, Center for Sustainability and the Global Environment, University of Wisconsin, Madison, WI 53726, USA. (eungul.lee@gmail.com)